High dietary fat and sucrose result in an extensive and time-dependent deterioration in health of multiple physiological systems in mice

Received for publication, November 14, 2017, and in revised form, February 12, 2018 Published, Papers in Press, February 13, 2018, DOI 10.1074/jbc.RA117.000808

James G. Burchfield[‡§1], Melkam A. Kebede[‡1], Christopher C. Meoli[‡§1], Jacqueline Stöckli[‡§], P. Tess Whitworth[§], Amanda L. Wright[§2], Nolan J. Hoffman[‡§3], Annabel Y. Minard[‡§4], Xiuquan Ma[§], James R. Krycer[‡§5], Marin E. Nelson[‡], Shi-Xiong Tan[§6], Belinda Yau[‡], Kristen C. Thomas[‡§], Natalie K. Y. Wee[§], Ee-Cheng Khor[§], Ronaldo F. Enriquez[§], Bryce Vissel[§7], Trevor J. Biden[§], Paul A. Baldock[§8], Kyle L. Hoehn[§9], James Cantley[§10], Gregory J. Cooney[‡¶], David E. James[‡§¶11], and Daniel J. Fazakerley[‡§]

From the [‡]Charles Perkins Centre, School of Life and Environmental Sciences, University of Sydney, Camperdown, New South Wales 2006, Australia, [§]Garvan Institute of Medical Research, Darlinghurst, Sydney, New South Wales 2010, Australia, and [¶]Charles Perkins Centre, Sydney Medical School, University of Sydney, Camperdown, New South Wales 2006, Australia

Edited by Jeffrey E. Pessin

Obesity is associated with metabolic dysfunction, including insulin resistance and hyperinsulinemia, and with disorders such as cardiovascular disease, osteoporosis, and neurodegeneration. Typically, these pathologies are examined in discrete model systems and with limited temporal resolution, and whether these disorders co-occur is therefore unclear. To address this question, here we examined multiple physiological systems in male C57BL/6J mice following prolonged exposure to a high-fat/high-sucrose diet (HFHSD). HFHSD-fed mice rapidly exhibited metabolic alterations, including obesity, hyperleptinemia, physical inactivity, glucose intolerance, peripheral insulin resistance, fasting hyperglycemia, ectopic lipid deposition, and bone deterioration. Prolonged exposure to HFHSD resulted in morbid obesity, ectopic triglyceride deposition in liver and muscle, extensive bone loss, sarcopenia, hyperinsulinemia, and impaired short-term memory. Although many of these defects are typically associated with aging, HFHSD did not alter telomere length in white blood cells, indicating that this diet did not generally promote all aspects of aging. Strikingly, glucose homeostasis was highly dynamic. Glucose intolerance was evident in HFHSD-fed mice after 1 week and was maintained for 24 weeks. Beyond 24 weeks, however, glucose tolerance improved in HFHSD-fed mice, and by 60 weeks, it was indistinguishable from that of chow-fed mice. This improvement coincided with adaptive β-cell hyperplasia and hyperinsulinemia, without changes in insulin sensitivity in muscle or adipose tissue. Assessment of insulin secretion in isolated islets revealed that leptin, which inhibited insulin secretion in the chow-fed mice, potentiated glucose-stimulated insulin secretion in the HFHSD-fed mice after 60 weeks. Overall, the excessive calorie intake was accompanied by deteriorating function of numerous physiological systems.

This work was supported in part by National Health and Medical Research Council of Australia Project Grants 1061122, 1086850 and 1086851 (to D. E. J.) and an Australian post-graduate award (to C. C. M., P. T. W., A. Y. M., A. L. W., and N. K. W.). The authors declare that they have no conflicts of interest with the contents of this article.

[1] These authors contributed equally to this work.
[2] Present address: Centre for Motor Neuron Disease Research, Dept. of Biomedical Sciences, Faculty of Medicine, Macquarie University, Sydney, New South Wales 2109, Australia.
[3] Present address: Centre for Exercise and Nutrition, Mary MacKillop Institute for Health Research, Australian Catholic University, Melbourne, Victoria 3000, Australia.
[4] Present address: Dept. of Molecular Physiology and Biophysics, University of Iowa, Iowa City, IA 52242.
[5] Supported by a National Health and Medical Research Council of Australia Early Career Fellowship.
[6] Present address: School of Applied Science, Republic Polytechnic, 738964 Singapore.
[7] Present address: Centre for Neuroscience and Regenerative Medicine, Faculty of Science, University of Technology Sydney, Sydney, New South Wales 2007, Australia.
[8] Australian Research Council Future Fellow.
[9] Present address: School of Biotechnology and Biomedical Sciences, University of New South Wales, Sydney, New South Wales 2052, Australia.
[10] Present address: Dept. of Physiology, Anatomy and Genetics, University of Oxford, Oxford OX1 2JD, United Kingdom.
[11] National Health and Medical Research Council of Australia Senior Principal Research Fellow. To whom correspondence should be addressed: D-17 Charles Perkins Centre, University of Sydney, Camperdown, New South Wales 2006, Australia. Tel.: 61-2-8627-5731; E-mail: david.james@sydney.edu.au.

Excessive consumption of calories is associated with deterioration of a range of physiological systems. Although the impact of specific macronutrients *per se* on health is highly debated, it is clear that diets enriched in sugar and fat result in obesity. It is widely recognized that obesity is a major risk factor for numerous diseases, including type 2 diabetes, cardiovascular disease, and at least nine types of cancer (1). Hence, the epidemic of obesity spreading throughout the world represents one of the major challenges for future human health.

Extensive studies in rodent models have shown that exposure to diets that resemble those commonly consumed by humans in modernized societies leads to a marked deterioration in a range of metabolic systems (2). Presumably due to enhanced palatability and/or different macronutrient compositions (*i.e.* protein, carbohydrate, and fat ratios) (3), diets high in sugar and/or a range of fats, including both saturated and polyunsaturated fats, invariably lead to excess calorie intake and drive animals toward a positive energy balance concomitant with obesity. This transition is associated with a rapid decline in whole-body

insulin sensitivity (4) ultimately resulting in compensatory hyperinsulinemia (4) and a state that resembles pre-diabetes in humans. Numerous laboratories have recapitulated these findings, and such diet-induced obesity models are widely used to study numerous facets of metabolic homeostasis and disease. For example, a high-fat high-sucrose diet (HFHSD)[12] feeding in mice is accompanied by alterations in circadian rhythm (5), gut microbiome (6), and inflammation (7), and these changes have been linked to metabolic dysfunction.

Aside from its obvious role in metabolic disease, obesity is also linked to a range of other diseases. There is evidence implicating obesity and Western diets high in saturated fats and refined sugars in the development of musculoskeletal (8, 9), pulmonary (10), kidney (11), and neurological (12, 13) disorders. However, most studies involve analysis of one physiological system in isolation often with limited time resolution. Hence, there is a need for a temporal systematic analysis of multiple physiological parameters in one or more of these diet-induced obesity models to fully realize the overall impact of obesity on health as well as the temporal relationship between impairments in distinct tissues.

In this study, we performed a comprehensive longitudinal analysis of the impact of HFHSD on a range of physiological systems in male C57BL/6J mice. We observed a time-resolved deterioration in the function of a multitude of physiological systems as mice became obese, including torpor, sarcopenia, bone loss, neurological dysfunction, as well as a range of metabolic disorders, including hyperinsulinemia, insulin resistance, glucose intolerance, and hepatic steatosis. Many of these effects emerged in a time-dependent manner, either occurring rapidly, such as bone loss, or more slowly, such as impaired short-term memory. The most complex set of adaptations was observed in glucose tolerance. HFHSD-fed mice displayed rapid glucose intolerance and insulin resistance. These changes persisted almost unchanged for 24 weeks after which glucose intolerance, but not insulin resistance, gradually improved and was ultimately resolved. This improvement was concomitant with increased β-cell mass and augmented circulating insulin concentrations. Leptin, which has previously been shown to suppress glucose-stimulated insulin secretion in islets, had the opposite effect in islets isolated from mice fed a HFHSD for 60 weeks, suggesting that islet responses to leptin are dependent on dietary context, and under these conditions leptin may promote insulin secretion *in vivo*. Our analysis provides a comprehensive assessment of the temporal adaptations to excess calorie intake in a host of physiological systems, highlights the pervasive effects of diet in multiple tissues, and lays the groundwork for further studies into the interaction between diet and health.

[12] The abbreviations used are: HFHSD, high-fat high-sucrose diet; BMC, bone mineral content; BMD, bone mineral density; GSIS, glucose-induced insulin secretion; GTT, glucose tolerance test; RER, respiratory exchange ratio; μCT, micro-computed tomography; DMEM, Dulbecco's modified Eagle's medium; 2-DOG, 2-deoxyglucose; EDL, Extensor digitorum longus; qPCR, quantitative PCR; Aβ, β-amyloid peptide; GIP, gastric inhibitory polypeptide; ROI, region of interest; HFD, high-fat diet.

Results

To dissect the temporal dynamics of metabolic, skeletal, and neurological responses to diet, we assessed indices of health in these systems in mice fed a control chow diet or HFHSD for 60 weeks as a model of diet-induced obesity. At 60 weeks, HFHSD-fed mice consumed ~34% more energy per day (3.1 kcal/g for chow; 4.7 kcal/g for HFHSD) (Fig. 1, *A* and *B*) indicating that increased calorie intake in mice fed HFHSD was maintained throughout the feeding period. As expected, chow-fed mice consistently displayed a higher respiratory exchange ratio (RER), indicating predominant use of carbohydrates in both the light and dark cycles at all time points studied (Fig. 1*C*). RERs were lower in HFHSD-fed mice and were lowered further with increasing time on the diet. This implies both an initial switch to fat as the major energy source and continued adaptation to further increase fat use (Fig. 1*C*). We also observed a significant reduction in the activity of mice fed HFHSD after only 6 weeks, and this was maintained for the duration of the HFHSD feeding (Fig. 1*D*). Hence, HFHSD-fed mice consumed additional calories and were less physically active, placing these animals in a state of positive energy balance.

Not surprisingly, the positive energy balance observed in HFHSD-fed mice resulted in gradual and profound increases in body mass (Fig. 1*E*) and obesity. Adiposity was not changed in chow-fed mice over the course of 60 weeks, but it rapidly increased in HFHSD-fed mice, plateauing after 40 weeks (Fig. 1*F*). We also measured distinct temporal patterns of ectopic triglyceride deposition in liver, quadriceps muscle, and heart (Fig. 1*G*). Triglycerides were elevated in quadriceps after 6 weeks of HFHSD feeding, and this was sustained for 60 weeks. In contrast, increased levels of triglycerides were only observed in liver at 24 weeks and in heart at 60 weeks (Fig. 1*G*). The major increase in triglyceride in muscle and liver was measured at 24 weeks of HFHSD and was concomitant with the plateau in adiposity (Fig. 1*F*), suggesting a link between adipose storage capacity or maximum adiposity and ectopic lipid deposition. Lean mass was not different between diet groups across the time course (Fig. 1*H*), while after 24 weeks of exposure to the diets, HFHSD-fed mice, but not chow-fed mice, displayed a 15% decline in mass of some specific muscles indicative of accelerated sarcopenia at these sites (Fig. 1*I*). Overall, mice fed a HFHSD displayed increased caloric intake, lower physical activity, and increased adiposity and body mass, providing a good model for the pathogenesis of diet-induced obesity in humans.

High-fat high-sucrose diet feeding rapidly lowers bone density and strength

We next examined the temporal changes in a range of physiological systems in the HFHSD-fed mice as diet has been reported to have pervasive effects on health. For example, individuals with insulin resistance or diabetes have a higher incidence of bone fracture (14, 15) and Alzheimer's disease (16), suggesting that obesity may affect these physiological systems in addition to metabolism. Therefore, we next tested how HFHSD acutely and chronically influenced skeletal and neurological health.

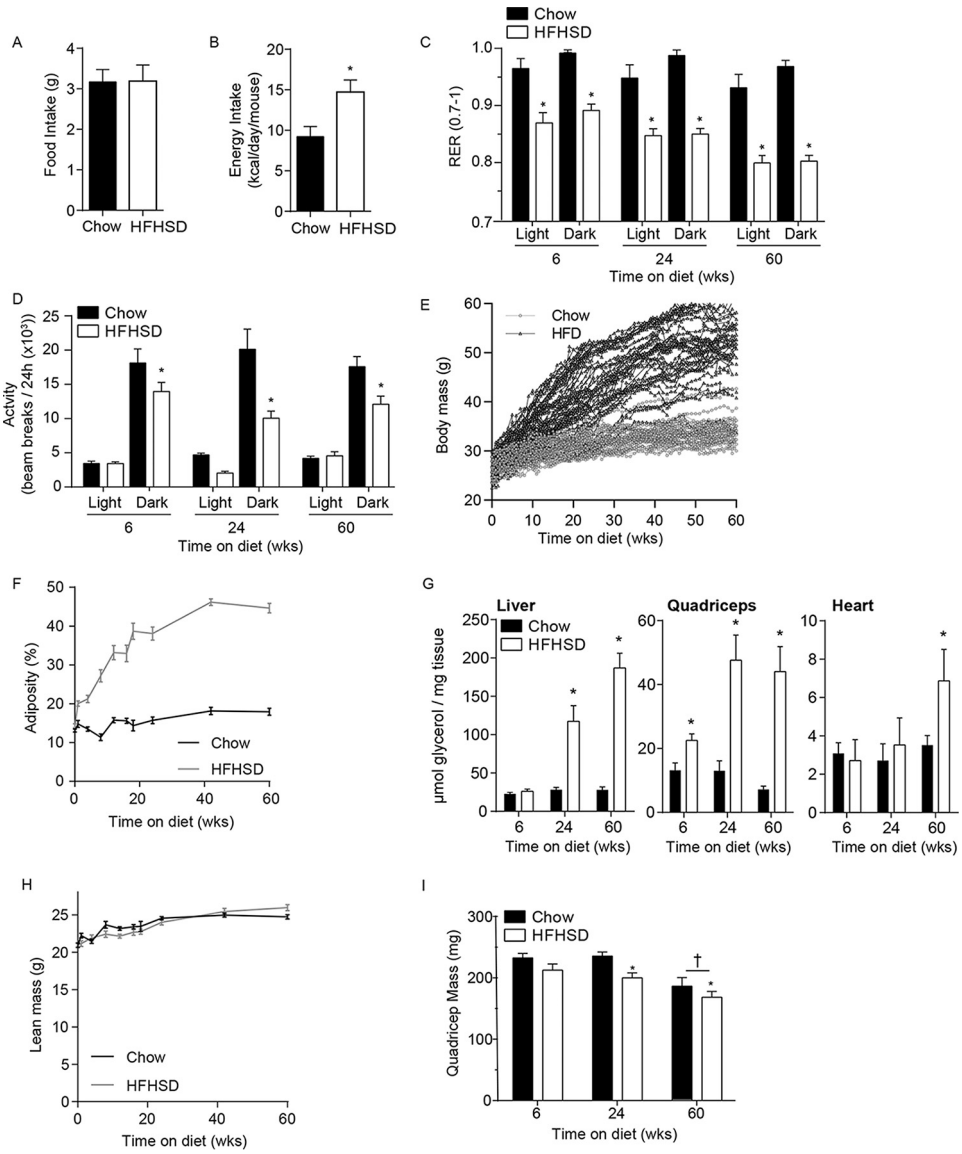

Figure 1. High-fat high-sucrose diet increases body weight and adiposity. *A* and *B*, food intake (*A*) was measured after 60 weeks of either chow (*black bars*) or HFHSD (*white bars*) feeding, and daily energy intake (kcal/day/mouse) was calculated (*B*). Data are mean ± S.E., Mann-Whitney, $n = 7$ chow-fed and $= 8$ HFHSD mice, *, $p < 0.05$ *versus* chow-fed controls. *C* and *D*, respiratory exchange ratios (*C*) and activity (number of beam crosses within 24 h) (*D*) were assessed in mice fed chow or a HFHSD for the indicated times (*wks* = weeks). Data were separated in to light and dark cycles. Data are mean ± S.E., $n = 4$ chow-fed and HFHSD for 6 weeks, 4 chow-fed and HFHSD for 24 weeks, and 8 chow-fed and HFHSD for 60 weeks, and *t* tests were corrected for multiple comparisons, *, $p <$ 0.05 *versus* age-matched chow-fed controls. *E* and *F*, body mass $n = 28–54$ mice for chow-fed and 27–54 for HFD (*E*) and percentage adiposity, $n = 8–24$ mice for chow-fed and 10–31 for HFHSD (*F*) of mice fed a chow (*black line*) or a HFHSD (*gray line*) for the indicated times. *G*, triglyceride content in liver, quadriceps, and heart tissue from mice fed a chow or a HFHSD for indicated times, $n = 9–23$ for quadriceps, 9–10 for liver, and 3–9 for heart. *H* and *I*, total lean mass, $n =$ 28–54 for chow-fed mice and 27–54 for HFHSD mice (*H*), and quadriceps mass, $n = 9–10$ (*I*), in mice fed a chow or HFHSD for indicated times. Data are mean ± S.E., *t*-tests corrected for multiple comparisons (*G* and *I*), *, $p < 0.05$, *versus* chow-fed age-matched controls; †, $p < 0.05$ *versus* mice fed either diet for 6 weeks (*I*).

Aging is associated with several bone diseases. Consistent with this, chow-fed mice displayed an age-related decline in bone mineral content (BMC) and bone mineral density (BMD) between 24 and 60 weeks of the study (Fig. 2, *A* and *B*). This loss was exacerbated at 24 and 60 weeks in HFHSD-fed mice (Fig. 2, *A* and *B*). These differences were not related to changes in bone area or femur length (Fig. 2, *C* and *D*). We next assessed the microstructure of the distal femoral metaphysis by μCT scanning. Trabecular bone volume (Fig. 2, *E* and *M–R*) and trabecular number (Fig. 2, *F* and *M–R*) decreased with age in both chow- and HFHSD-fed mice. In addition, by 6 weeks HFHSD-fed mice had 33% less trabecular bone volume (Fig. 2*E*) and a 25% less trabecular number compared with age-matched chow-fed mice (Fig. 2*F*). Consistent with these observations, trabecular separation increased with age and was significantly greater in HFHSD-fed mice (Fig. 2*G*). Age had no effect on trabecular thickness in chow-fed mice (Fig. 2*H*), but trabecular thickness was increased at 24 weeks in HFHSD-fed mice but returned to baseline levels after 60 weeks (Fig. 2*H*). In addition, we detected age-related changes in cortical bone volume (Fig. 2*I*) and thickness (Fig. 2*J*), periosteal (Fig. 2*K*) and endosteal perimeters (Fig. 2*L*), and bone strength (polar moment of inertia) (Fig. 2*S*), but these parameters were not affected by diet, despite markedly greater weight in HFHSD-

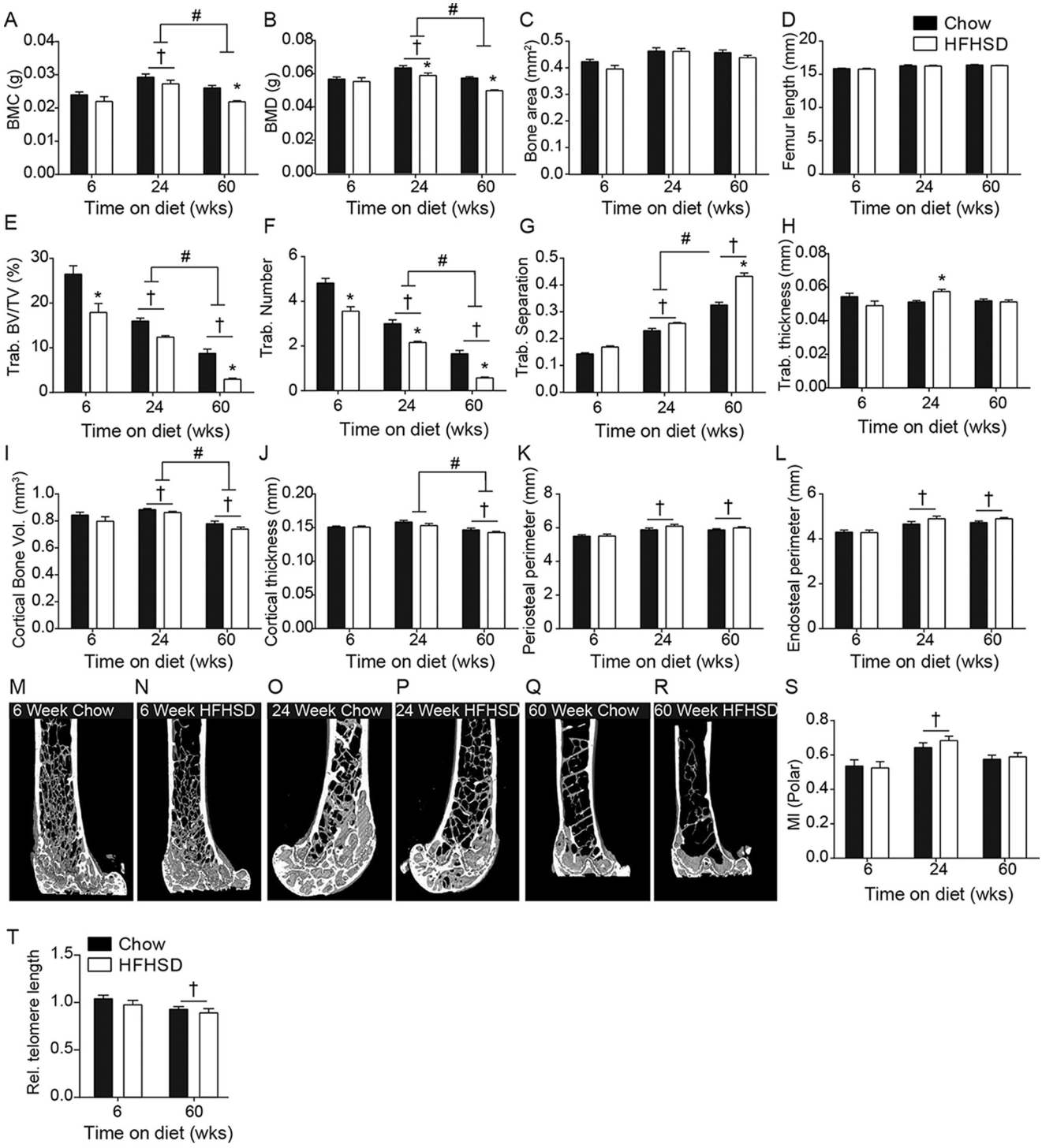

Figure 2. High-fat high-sucrose diet rapidly impairs skeletal structure. *A–C,* femora were isolated from mice fed chow (*black bars*) or HFHSD (*white bars*) for 6, 24, and 60 weeks (*wks*) and DEXA scanning utilized to measure femoral bone mineral content (BMC) (*A*), bone mineral density (BMD) (*B*), and bone area (*C*). *D,* length of femurs from mice fed chow or HFHSD for indicated times. *E–H,* μCT scanning of tarbecular bone from mice fed chow or HFHSD for indicated times assessed trabecular bone volume/total volume (*E*), trabecular number (*F*), trabecular separation (*G*), and trabecular thickness (*H*). *I* and *J,* cortical bone from mice fed chow or HFHSD for indicated times was assessed for cortical bone volume (*I*) and cortical thickness (*J*). *K* and *L,* periosteal (*K*) and endosteal (*L*) perimeters were measured from mice fed chow or HFHSD for indicated times. *M–R,* representative images showing the loss in trabecular bone volume and trabecular number and changes in cortical thickness in mice fed chow or HFHSD for 6 (*M* and *N*), 24 (*O* and *P*), and 60 (*Q* and *R*) weeks, respectively. *S,* polar moment of inertia (was calculated using the Skyscan CT analyzer software as an indicator of bone strength in isolated femurs. *T,* relative telomere length in mice fed a chow or HFHSD for 6 or 60 weeks. Data are mean ± S.E., $n = 10$, 10, and 18 mice per group for 6, 12, and 60 weeks, respectively; *t* tests corrected for multiple comparisons;*, $p <$ 0.05 *versus* age-matched chow; †, $p < 0.05$ *versus* mice fed either diet for 6 weeks; #, $p < 0.05$ *versus* mice fed either diet for 24 weeks as indicated.

fed mice (Fig. 1*E*). Together, these data show that HFHSD feeding has a rapid and profound effect on bone microstructure without significant effects on cortical bone or bone strength. Specifically, HFHSD feeding appeared to worsen the age-related decline in trabecular bone, BMC, and BMD.

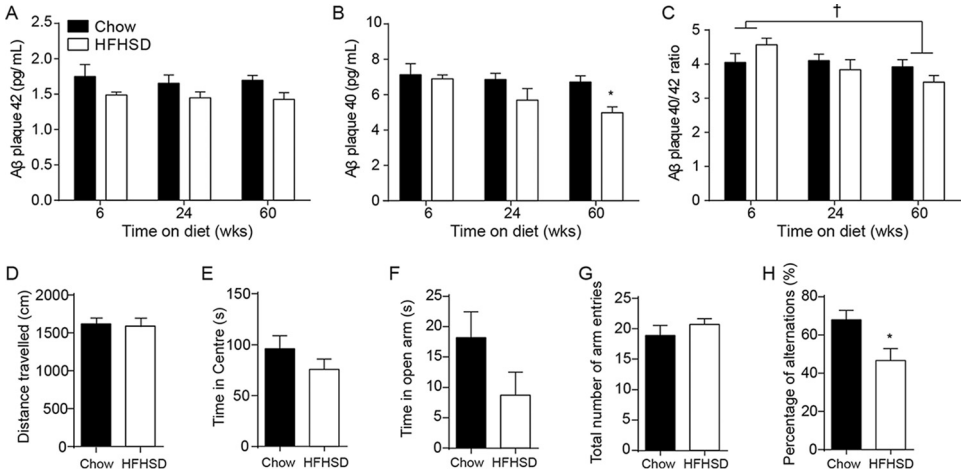

Figure 3. Prolonged high-fat high-sucrose diet feeding impairs short term memory. *A–C,* hippocampal Aβ 42 (*A*) and 40 (*B*) were measured and the Aβ-40/42 ratio calculated for mice fed a chow (*black bars*) or HFHSD (*white bars*) for indicated times (weeks = weeks) (*C*). *D–H,* mice fed a chow or HFHSD for 60 weeks were subjected to the open field test (*D* and *E*), elevated plus-maze (*F*), and Y-maze (*G* and *H*). The open field test provided a measure of locomotion (*D*) and anxiety as measured by time in the center of the apparatus (*E*). *F,* elevated plus-maze directly measured anxiety by quantifying time in open arms of the maze. *G* and *H,* Y-maze provided a measured of activity (*G*) by measuring number of entries into arms of the maze and short term spatial memory by quantifying the number of entries into alternate arms of the maze (alternations) (*H*). Data are mean ± S.E., $n = 5$ per group for 6- and 24-week-old mice, $n = 8$ for 60-week chow-fed and $n = 11$ for 60-week HSHFD mice. *t* tests corrected for multiple comparison; *, $p < 0.05$ *versus* age matched chow; †, $p < 0.05$ *versus* mice fed either diet for 6 weeks as indicated.

High-fat high-sucrose diet feeding did not alter leukocyte telomere length

Because obesity exacerbated the age-dependent decline in bone microarchitecture, we next tested whether HFHSD-fed mice exhibited signs of increased biological age *per se*. To do this, we assessed telomere length in white blood cells. As expected, telomere length decreased with age (Fig. 2*T*), but this decline was unaffected by diet. This suggests that HFHSD did not generally promote all aspects of aging and that the association found between obesity and age-related loss in bone quality is rather due to specific effects on bone.

Prolonged high-fat high-sucrose diet feeding impairs short-term memory

To assess brain health and cognitive function, we first assessed molecular markers of neurodegenerative disease susceptibility. Alzheimer's disease and related neurodegenerative diseases are strongly associated with the formation of fibrillary plaques in the brain. The major components of these plaques are forms of β-amyloid peptide (Aβ), Aβ40 and Aβ42, that are generated by proteolytic cleavage of amyloid precursor protein. Hippocampal Aβ42 content was not changed by age or diet (Fig. 3*A*), but HFHSD-fed mice exhibited lower levels of the protective Aβ40 after 60 weeks compared with age-matched chow-fed controls (Fig. 3*B*). Despite lower Aβ40 content, we detected no difference in the Aβ-40/42 ratio between diets, although the Aβ-40/42 ratio decreased with age when both diet groups were considered together (Fig. 3*C*).

Neurodegenerative diseases result in behavioral alterations, including depression, anxiety, and loss of short-term memory (17, 18). We next tested whether HFHSD impaired locomotion, anxiety, or short-term memory. We first performed an Open Field Test as a measure of general activity and observed that diet had no impact on total distance traveled (Fig. 3*D*) or anxiety, as determined by the time spent in the center of the apparatus (Fig. 3*E*). Similar results were obtained when the mice were placed in an Elevated Plus Maze, a more specific test for anxiety (Fig. 3*F*). The Y-Maze Test assesses short term working memory by measuring spontaneous alternation within the maze. No difference was observed in the total number of arm entries between chow- and HFHSD-fed mice (Fig. 3*G*) suggesting that all mice had the same level of motivation, curiosity, and motor function. However, the percentage of alternations was lower in HFHSD-fed mice, indicative of a short-term working memory deficit (Fig. 3*H*). These data indicate that long-term HFHSD feeding impaired short-term memory in mice concomitant with a decrease in the protective Aβ40 peptide in the brain.

Prolonged high-fat high-sucrose diet feeding overcomes glucose intolerance

To assess the impact of HFHSD feeding on glucose metabolism, we monitored fed and fasting glucose concentrations and glucose tolerance periodically throughout the 60-week dietary intervention. Post-prandial blood glucose concentrations did not differ between the diet groups across the 60-week time course (Fig. 4*A*), but fasting blood glucose concentrations were elevated in HFHSD-fed mice from 8 to 52 weeks, after which they returned to chow levels (Fig. 4*B*). As expected, glucose intolerance was evident in HFHSD-fed mice after 1 week on the diet (Fig. 4*C*). This same degree of glucose intolerance was maintained for 24 weeks (Fig. 4, *C* and *D*). Surprisingly, mice fed a HFHSD for more prolonged periods (40–60 weeks) had marked improvements in glucose tolerance compared with those fed the diet for 1–32 weeks when accounting for differences in basal glucose (Fig. 4, *C* and *D*). Over the 60-week time course, chow-fed mice did not exhibit changes in fasting or fed glucose levels or glucose tolerance (Fig. 4, *A–D*).

To examine whether improved glucose tolerance in HFHSD-fed mice was associated with improved peripheral insulin sensitivity, we next measured insulin-stimulated 2-deoxyglucose

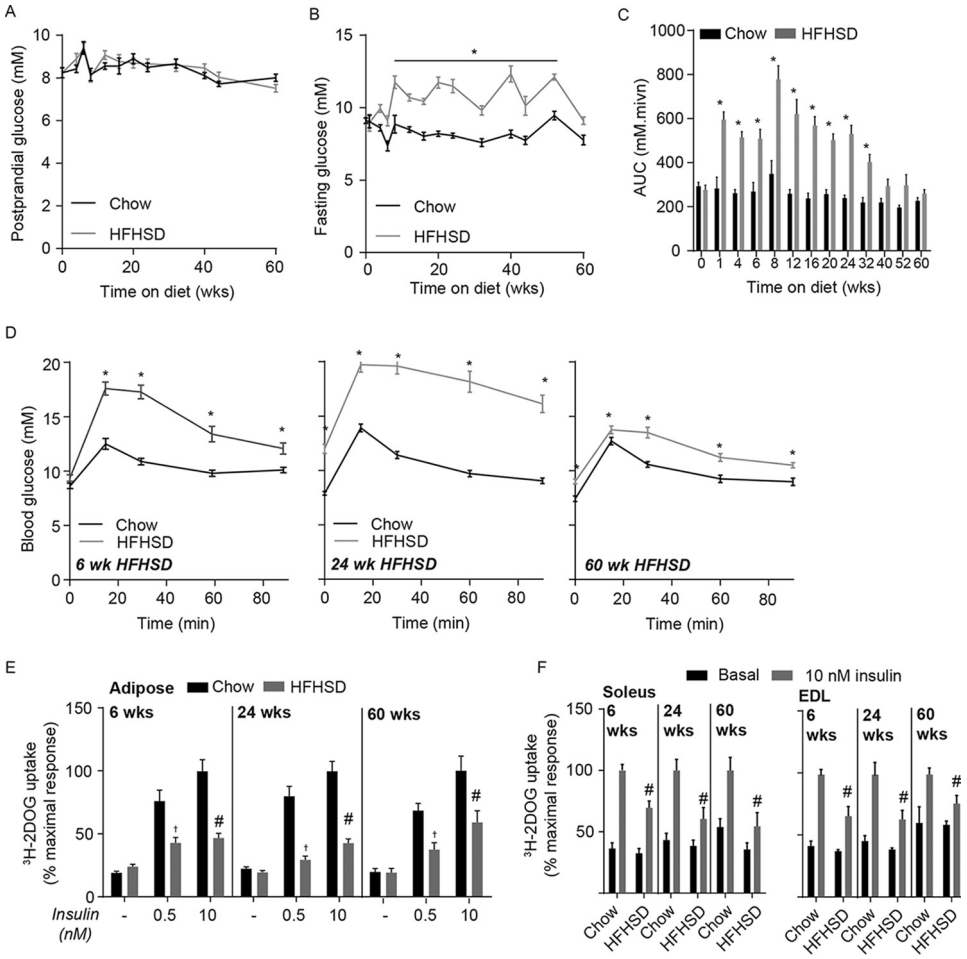

Figure 4. Glucose tolerance in high-fat high-sucrose diet fed mice resolves with prolonged exposure to high-fat high-sucrose diet. *A* and *B,* postprandial (*A*), $n = 18–41$ and fasting (*B*), $n = 10–30$, blood glucose concentrations in mice fed a chow (*black line*) or HFHSD (*gray line*) for indicated times (*wks* = weeks). Data are mean ± S.E., *t* tests corrected for multiple comparisons; *, $p < 0.05$ *versus* chow-fed controls. *C,* area under the curve calculated from blood glucose concentrations during glucose tolerance tests in mice fed a chow (*black bars*) or HFHSD (*gray bars*) for indicated times. Data are mean ± S.E., $n = 7–42$; *t* tests corrected for multiple comparisons; *, $p < 0.05$ *versus* chow-fed age-matched controls. *D,* representative blood glucose concentrations during a glucose tolerance test in C57BL/6J mice fed a chow or HFHSD for 6, 24, or 60 weeks. Data are mean ± S.E., $n = 20–25$ at 6 weeks, 38–39 at 24 weeks, 20–26 at 60 weeks, *t* tests corrected for multiple comparisons, *, $p < 0.05$ *versus* chow-fed controls. *E,* rates of 2-[^{3}H]DOG uptake into epididymal adipose explants from mice fed a chow or HFHSD for 6, 24, or 60 weeks under unstimulated conditions and in response to 0.5 or 10 nM insulin. Data are mean ± S.E., $n = 4–10$, *t* tests corrected for multiple comparisons; †, $p < 0.05$ *versus* 0.5 nM insulin chow mice; #, $p < 0.05$ *versus* 10 nM insulin chow mice. *F,* rates of 2-[^{3}H]DOG uptake into isolated soleus muscles (*left panel*) or EDL (*right panel*) muscles from mice fed a chow or HFHSD for 6, 24, or 60 weeks under unstimulated conditions (basal) and in response 10 nM insulin. Data are mean ± S.E., $n = 5–14$, *t* tests corrected for multiple comparisons;, #, $p < 0.05$ *versus* 10 nM chow.

uptake into white adipose tissue and skeletal muscle *ex vivo*. Insulin-dependent 2-deoxyglucose uptake was significantly reduced in both adipose tissue and muscles from HFHSD-fed mice after 6 weeks of feeding, and both tissues remained similarly insulin-resistant for the duration of the time course (Fig. 4, *E* and *F*). This is in line with the decreased RER (Fig. 1*C*) we observed in mice fed HFHSD, which may be attributed to preferential use of fatty acid over glucose for energy. Therefore, the improved glucose tolerance observed at 60 weeks of HFHSD did not correspond to improved insulin sensitivity in peripheral tissues.

Improved glucose tolerance coincides with hyperinsulinemia

To further investigate possible mechanisms behind long-term improvements in glucose tolerance in HFHSD-fed mice, we assessed the circulating concentrations of key metabolic hormones. As expected, leptin concentrations correlated with adiposity and were already increased after only 6 weeks of HFHSD feeding (Fig. 5*A*). Similarly, GIP was elevated in HFHSD-fed mice at all time points (Fig. 5*D*), whereas interleukin-6 (IL6) was increased only after 60 weeks, and resistin levels were not significantly altered (Fig. 5, *B* and *C*). Therefore, HFHSD feeding affected most of these selected metabolic hormones, and the rise in GIP, a known incretin, is of interest given its role in enhancing insulin secretion and β-cell proliferation. Indeed, longitudinal analysis of circulating insulin levels over 60 weeks of HFHSD feeding revealed increased fasting and postprandial insulin levels starting from 12 weeks and plateauing at 40 weeks (Fig. 5, *E* and *F*). These time points correspond with the onset of improved glucose tolerance (Fig. 4, *C* and *D*), implying that compensatory β-cell-enhanced responsiveness may contribute to normalization of glucose tolerance.

β-Cell proliferation and adipose expansion within pancreata correlates with hyperinsulinemia

Increased circulating insulin can be driven by decreased insulin clearance, increased insulin secretion per β-cell, and/or

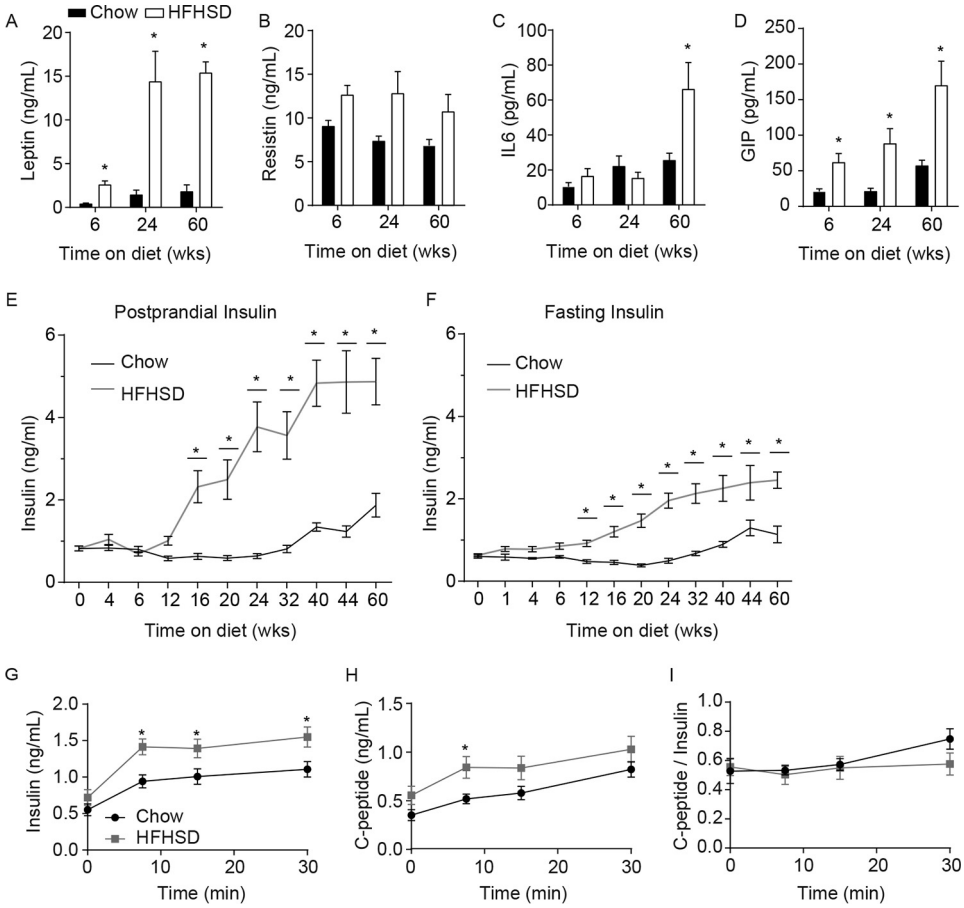

Figure 5. Prolonged high-fat high-sucrose diet feeding induces hyperinsulinemia. *A–D,* concentrations of leptin (*A*), resistin (*B*), IL6 (*C*), and gastric inhibitory polypeptide (*GIP*) (*D*) in serum from mice fed a HFHSD (*white bars*) for indicated times and chow-fed controls (*black bars*) (*wks* = weeks). Data are mean ± S.E., $n = 4–12$, *t* tests corrected for multiple comparisons; *, $p < 0.05$ *versus* chow-fed controls. Postprandial (*E*) and fasting (*F*) circulating insulin levels in mice fed a HFHSD (*gray line*) for specified times and chow-fed controls (*black line*) are shown. Data are mean ± S.E., $n = 7–30$, *t* tests corrected for multiple comparisons; *, $p < 0.05$ *versus* chow-fed controls. *G–I,* circulating insulin (*G*) and C-peptide (*H*) concentrations during an i.p. GTT following an overnight fast in mice fed chow or HFHSD for 60 weeks. The C-peptide/insulin ratio (*I*) was calculated from *G* and *H*. Data are mean ± S.E., $n = 8–9$, *t* tests corrected for multiple comparisons, *, $p < 0.05$ *versus* chow-fed controls.

increased β-cell mass. Insulin clearance, as measured by the C-peptide to insulin ratio, was not affected in HFHSD-fed mice after 60 weeks of feeding (Fig. 5, *G–I*). Therefore, we next examined how HFHSD feeding influenced pancreatic morphology and islet number (Fig. 6*A*). Pancreas mass was decreased by ~33% at 60 weeks of HFHSD feeding (Fig. 6*B*), and the pancreas area showed a similar trend (Fig. 6*C*). Despite decreased pancreas mass (Fig. 6*B*), the total number of islets remained constant (Fig. 6*D*). Given the increase in average islet area (Fig. 6, *E* and *F*), this suggests an increase in total β-cell mass. This was associated with a transient increase in Ki67-positive cells at 24 weeks (Fig. 6*G*), suggesting that the increase in β-cell mass was likely driven by increased β-cell proliferation. Therefore, increased β-cell mass likely contributes to the progressive hyperinsulinemia observed in mice fed the HFHSD.

Hyperinsulinemia is not due to greater basal insulin secretion per β-cell

Analysis of insulin secretion during an i.p. GTT revealed greater insulin secretion in HFHSD-fed mice at 60 weeks (Figs. 5*G* and 7*A*). Therefore, we next investigated β-cell function by examining glucose-stimulated insulin secretion (GSIS) in islets from chow-fed and HFHSD-fed mice (Fig. 7, *B–D*). We observed hypersecretion of insulin at 2 mM glucose and a reduced secretory response at 20 mM glucose in HFHSD-fed mice after 6–12 weeks on the diet. As the mice progressed on the HFHSD (>18 weeks), the secretory response normalized, such that by 60 weeks, islets from mice fed HFHSD responded similarly to chow-fed controls (Fig. 7, *C* and *D*). These data show that although HFHSD feeding induced an acute defect in GSIS, this was overcome at longer time points. Despite restored GSIS at longer HFHSD time points, these data from isolated islets do not support a sole role for an increased β-cell response to glucose in contributing to the progressive hyperinsulinemia in HFHSD-fed mice. Rather, they point to a role for increased β-cell mass and/or exposure to circulating factors such as GIP in augmenting circulating insulin concentrations.

High-fat high-sucrose diet alters islet responses to leptin

Our histochemical analysis revealed a pronounced proliferation of adipocytes in pancreata from HFHSD-fed mice (Fig. 6*H*). This reached a maximum at 24 weeks with adipocytes making up 5% of the total pancreas volume, and in some cases, islets were completely surrounded by adipocytes with no appar-

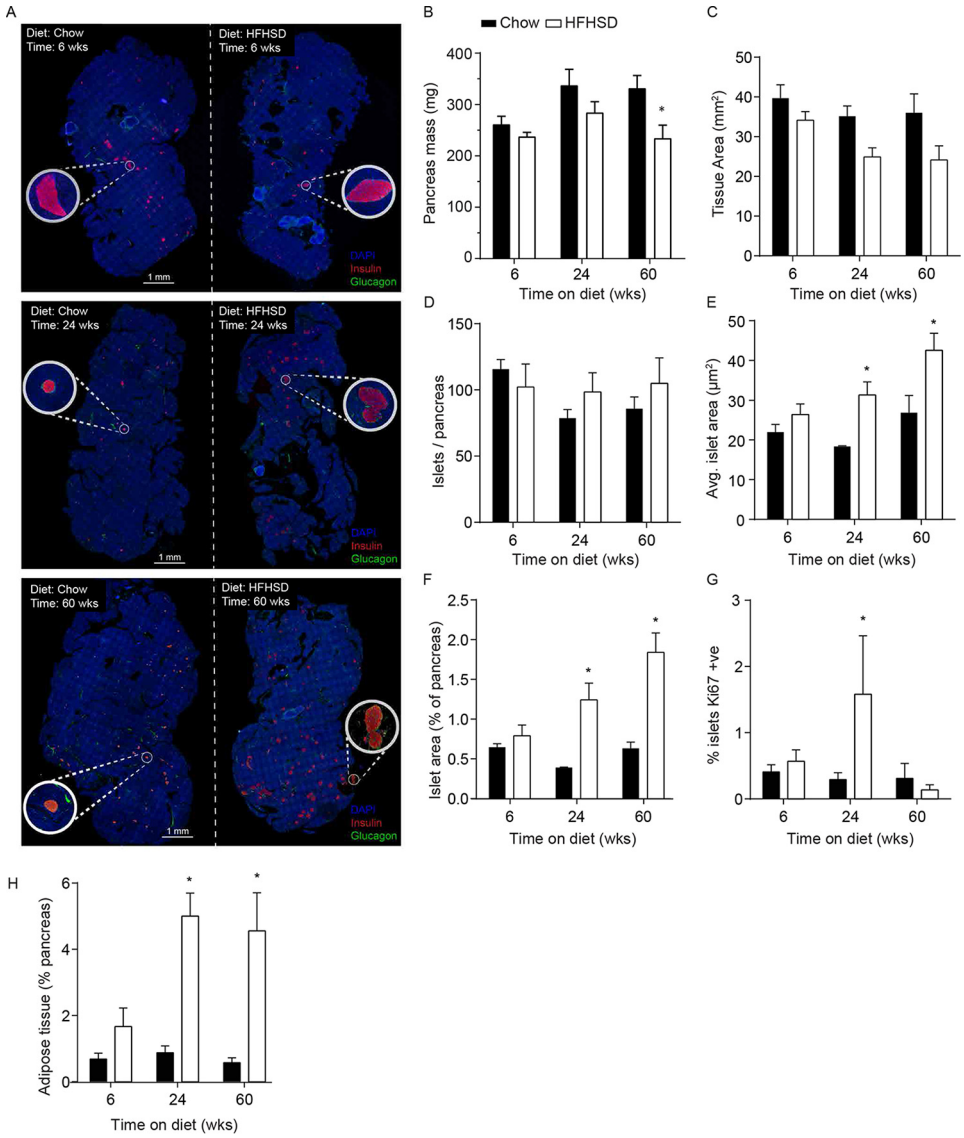

Figure 6. β-Cell hyperplasia in high-fat high-sucrose diet-fed mice. *A,* representative images of pancreatic slices from mice fed a HFHSD for indicated times (*wks* = weeks) and chow-fed controls stained for nuclei (DAPI, *blue*), insulin (*red*), and glucagon (*green*). *B,* pancreatic mass from mice fed chow (*black bars*) or HFHSD (*white bars*) for indicated times. Data are mean ± S.E., *t* tests corrected for multiple comparisons; *, $p < 0.05$ *versus* chow-fed controls. *C–F,* tissue area (*C*), number of islets per pancreas (*D*), average islet area (*E*), and islet area as a percentage of pancreas area (*F*) were calculated from pancreas images (*A*). Data are mean ± S.E., *t* tests corrected for multiple comparisons; *, $p < 0.05$ *versus* chow-fed controls. *G,* pancreatic sections were stained with Ki67 as a measure of cell proliferation, and Ki67-positive islets were quantified. *H,* adipocytes within pancreatic slices were quantified. Data are mean ± S.E., *t* tests corrected for multiple comparisons; *, $p < 0.05$ *versus* chow-fed control, $n = 4$ mice per group with three sections per pancreas.

ent cell-to-cell contact with acinar tissue (Fig. 6*A*, *lower panel, right inset*). Based on this observation and the fact the time course of this change coincided with the emergence of improved glucose tolerance in HFHSD mice, we surmised that the adaptive hyperinsulinemia may be due to a paracrine effect from local release of adipokines from pancreas-associated adipocytes. Based upon our profiling of circulating factors, the most likely candidate for this effect was leptin (Fig. 5*A*). Thus, we next examined the effect of leptin on GSIS *in vitro*. Consistent with the literature (19–21), leptin inhibited GSIS by ~30% in islets from chow-fed mice at all time points (Fig. 7*E*). Strikingly, leptin had no effect on GSIS in islets from HFHSD-fed mice for up to 32 weeks of feeding (Fig. 7*E*), indicative of leptin resistance, whereas leptin potentiated GSIS in mice fed a HFHSD for 60 weeks (Fig. 7*E*). Collectively, these data reveal a major effect of leptin to potentiate insulin secretion in the context of long-term calorie excess.

Discussion

This study provides a systematic insight into the effects of calorie excess on health. Marked deterioration of every physiological system examined was observed spanning skeletal muscle, liver, bone, brain, adipose tissue, and pancreas. Exposure of C57BL/6J mice to a HFHSD resulted in excess intake of calories, torpor, sarcopenia, hepatic steatosis, lipid accumulation in muscle, pancreas, and heart tissue, pre-diabetes, bone loss, and impaired neurological function. These findings represent some of the major diseases observed in aging humans, and so this extends previous studies to show that overconsumption of calories alone is a major risk factor for numerous diseases. The

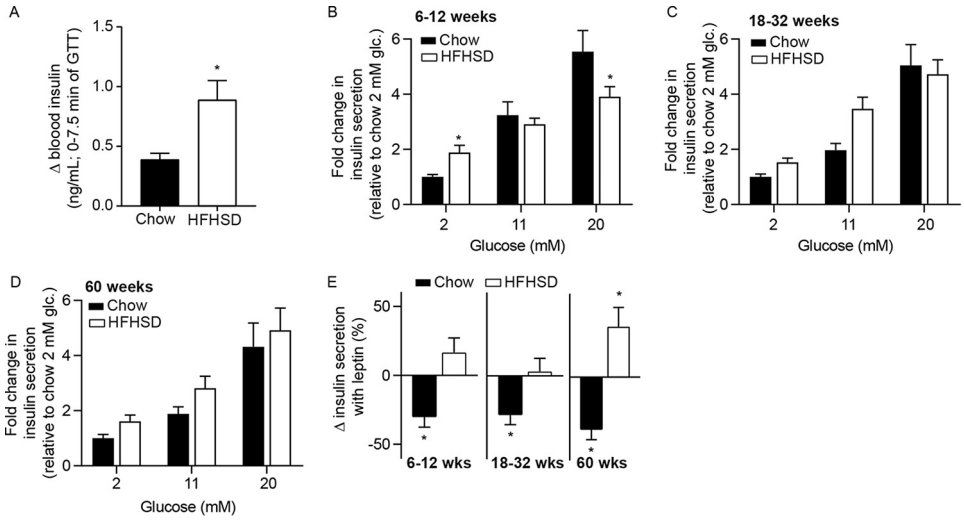

Figure 7. High-fat high-sucrose diet feeding switches islet responses to leptin. *A,* change in blood insulin concentration during the first 7.5 min of an i.p. GTT performed on mice fed chow (*black bars*) or HFHSD (*white bars*) for 60 weeks. Data were reanalyzed from Fig. 5*G*. Data are mean ± S.E., $n = 8–9$, Mann-Whitney with correction for multiple comparisons; *, $p < 0.05$ *versus* chow response. *B–D,* insulin secretion from primary islets isolated from mice fed chow or HFHSD for indicated times and incubated with 2, 11, or 20 mM glucose. Data from control mice and mice fed a HFHSD for 6 and 12 weeks (weeks) (*B*), 18, 24, and 32 weeks (*C*) were similar and so were combined for statistical power, whereas and data from control mice and mice fed a HFHSD for 60 weeks were analyzed as a single time point (*D*). Data are mean ± S.E., $n = 19$ at 6–12 weeks, 17 at 18–24 weeks, and 15 at 60 weeks; *t* tests corrected for multiple comparisons; *, $p < 0.05$ *versus* chow response at same glucose concentration. *E,* insulin secretion in response to 11 and 20 mM glucose was assessed in the presence of 20 ng/ml leptin. Percentage change in insulin secretion was calculated per mouse. Data are mean ± S.E., Wilcoxon signed-rank test to test for difference from 0, *, $p < 0.05$. $n = 16$ and 18 at 6–12 weeks; 23 and 18 at 18–32 weeks; 25 and 27 at 60 weeks for chow- and HSHFD-fed mice, respectively.

temporal onset of these disorders varied considerably in the mouse, and certain systems exhibited a complex dynamic adaptive response. This was most notable for the gluco-insular axis whereby animals rapidly developed glucose intolerance that was ultimately resolved in concert with adaptive hyperinsulinemia. The latter was partly due to β-cell hyperplasia as well as a novel stimulatory effect of leptin on insulin secretion. Given that these mice also displayed hyperleptinemia, it is conceivable that this leptin "switch" plays a role in β-cell compensation under these conditions.

It is noteworthy that aging to 60 weeks had limited effect on the metabolic indices measured in chow-fed control mice. This is despite the presence of a truncation mutation in the nicotinamide nucleotide transhydrogenase gene (22) in the C57BL/6J strain, which has been associated with glucose intolerance and insulin secretory dysfunction compared with mice without the *nnt* mutation (22). In agreement with other longitudinal studies (23–26), our analysis did not detect any significant changes in glucose tolerance, fasting or fed circulating insulin levels, 2-DOG glucose uptake into adipocytes, and muscle- or glucose-stimulated insulin secretion in these mice throughout the 60-week feeding period.

The effect of diet on a range of physiological systems has been extensively studied, and a number of reports have documented deleterious effects of high fat diets on skeletal (8, 9) and neurological function (12, 13). Many of these studies have been performed in isolation, and they often do not examine the temporal aspects of these perturbations. The strength of this study is that we provide a systematic temporal analysis of the consequences of diet-induced obesity on many physiological parameters in parallel. This is important as it lays the groundwork for a detailed longitudinal analysis of the interaction between diet and a range of other factors, including genetics, epigenetics, and early development. Such analyses are crucial as there is considerable interest in precision medicine in humans, yet proof-of-principle for such approaches in model systems like mouse is lacking. It is clear from this study that the mouse is a useful system to study the ontogeny of a host of diet-induced defects in health. Intriguingly, although we observed depreciation in a range of physiological systems as noted above, there was no evidence for obesity increasing biological age in general, because telomere length in white blood cells was unchanged in HFHSD-fed mice, suggesting that these were tissue-specific responses to diet. We also observed considerable differences in the temporal patterns in that certain defects like loss of trabecular bone occurred very rapidly, whereas other defects like loss of bone mineral content and density and impaired short-term memory occurred more slowly.

The advantage of these temporal distinctions is that it is possible to correlate these defects with changes in known modulators of bone and neurological health. For example, a number of factors, including activity, load, leptin, insulin, and IL6 are known to regulate bone health. Both insulin and leptin contribute to bone formation, and extensive investigations have shown that both insulin and leptin resistance play a role in bone loss associated with diet-induced obesity (27–29). IL6 enhances bone resorption (30). However, we only report evidence for lower activity and leptin and insulin resistance by 6 weeks of HFHSD feeding, when trabecular bone was compromised. Lower activity is known to decrease trabecular bone mass (31), and leptin has both a direct (32) and an indirect (33) effect on bone metabolism. In addition, high mechanical loading (weight) is a dominant stimulus of bone mass accretion, yet diet-induced obesity did not increase bone despite increasing body mass by ~20 g. Alarmingly, studies in mice have shown that diet-induced changes in bone health are persistent and

cannot be completely reversed upon removal of the HFHSD challenge (9). Hyperinsulinemia has been associated with progression to Alzheimer's disease (12, 13, 34–36). Accordingly, we detected changes in the Aβ40 isoform and cognitive impairment only after prolonged exposure to the diet and development of marked hyperinsulinemia. Given the link between diet and health indices in bone and brain, our findings further highlight the need to understand how diet, even short-term HFHSD consumption, and the associated metabolic adaptation, including hyperinsulinemia and hyperleptinemia, may affect the health of multiple organ systems in later life.

As described previously (23), glucose intolerance occurred very rapidly in response to HFHSD feeding, and this was associated with a decline in insulin action in both muscle and adipose tissue. However, our temporal analysis of HFHSD feeding revealed several novel features of this response. First, exactly the same degree of insulin resistance and glucose tolerance was maintained for 24 weeks on the diet with no evidence of a progressive deterioration in these systems over this time. This was despite a marked increase in muscle and liver triglyceride accumulation at 24 weeks of HFHSD feeding, which occurred at the same time that HFHSD-induced increases in adiposity plateaued. In fact, insulin resistance in muscle and fat was maintained at exactly the same level for the entire 60 weeks of the study. This indicates that the defect is not cumulative or graded, but rather it occurs very early after exposure to the diet in a switch-like manner. This is intriguing as adipose tissue inflammation, which occurs progressively in response to HFHSD feeding, was suggested to contribute to insulin resistance at later time points (37, 38). However, our data from *ex vivo* assays do not support deteriorating insulin responses in adipose or muscle, although we cannot rule out differing responses *in vivo*. It was of interest that insulin resistance was evident prior to the development of fasting or fed hyperinsulinemia in this study indicating that the latter may not be the principal driver of insulin resistance in HFHSD-fed mice. Decreased glucose uptake into adipose tissue and skeletal muscle could be attributed to preferential use of fatty acid over glucose for energy as seen with the decreased RER (Fig. 1*C*) in mice fed HFHSD.

Perhaps of most interest was the progressive resolution of glucose intolerance with prolonged HFHSD feeding, as observed previously (25). This was a very slow process and appears to require several discrete but overlapping changes, including expanded β-cell mass (39, 40) and restored insulin secretory function following an initial defect in insulin secretion upon transition to HFHSD (41, 42). However, we also observed a progressive change in the islet response to leptin, beginning with leptin resistance in islets as indicated by an inability of leptin to inhibit GSIS, as was the case in islets from chow-fed mice. At later time points on the HFHSD, we observed a potentiating effect of leptin on GSIS. Together, it is likely that increased circulating insulin in mice fed a HFHSD for >24 weeks is driven by a range of factors, including increased β-cell mass, restored β-cell secretory responses, and altered responses to circulating factors such as leptin, GLP1/GIP, and free fatty acids that act to enhance insulin secretion.

The relationship between leptin and insulin secretion is intriguing; whereas obesity causes both hyperinsulinemia and hyperleptinemia, leptin is reported to inhibit GSIS through a direct effect on K^+ATP channels (19) or indirectly via phosphatidylinositol 3-kinase–dependent activation of phosphodiesterase PDE3B (20). Therefore, leptin would be predicted to suppress hyperinsulinemia in obesity due to increased circulating leptin under these conditions. However, our data in isolated islets revealed leptin resistance in islets as early as 6 weeks of HFHSD feeding. This may be driven by desensitization to leptin because circulating leptin concentrations were elevated in HFHSD-fed mice at this time. The "switch" in leptin signaling after 60 weeks of HFHSD feeding is similar to the change in leptin signaling output reported in neuronal development (43), and it is in agreement with phenotypes of pancreas-specific leptin receptor knockout mice challenged with HFHSD (21) and in mice with deletion of the leptin receptor both in β-cells and hypothalamus (44). These mice develop obesity, fasting hyperinsulinemia, and impaired glucose-stimulated insulin secretion; consistent with a stimulatory role of leptin signaling on insulin secretion during obesity (45). Taken together with our observations, these data suggest that leptin exerts a different role on β-cell function depending on the nutritional context, and it will be of interest to understand the mechanism underlying this switch. It is tempting to speculate that the effect of leptin observed in *ex vivo* assays may be exacerbated *in vivo* through paracrine delivery of leptin from local adipose tissue within pancreata. Indeed, these intrapancreatic adipocytes that we observed in 60-week HFHSD-fed mice may also provide a local source of lipid intermediates and/or adipokines that are known to modulate GSIS. We have previously reported an effect of FABP4 released from adipocytes to potentiate insulin secretion in mice, and this could also contribute to the compensatory hyperinsulinemia (46). Overall, induction of leptin resistance at early time points of HFHSD feeding may prevent leptin-induced inhibition of GSIS and permit compensatory hyperinsulinemia. The later functional switch in leptin signaling may contribute to the restoration of glucose homeostasis observed at 60 weeks, given the hyperleptinemia and increased pancreatic adipose tissue at this time point.

Insulin-resistant humans often exhibit normal glucose tolerance due to increased insulin secretion (47, 48). This is distinct from acute responses to HFHSD in C57BL/6J mice, which become glucose-intolerant without hyperinsulinemia. In contrast, the metabolic phenotype measured in C57BL/6J mice fed a HFHSD for 42–60 weeks more closely mimics the human condition. Furthermore, the delayed adaptive response in insulin secretion to overcome insulin resistance in C57BL/6J mice allowed us to pinpoint factors that may contribute to increased insulin secretion, including a novel role of leptin in this process. The dynamics of increased insulin secretion in response to HFHSD may be determined by genetic background because other mouse strains more rapidly increase insulin secretion in response to HFHSD (49). It will be of interest to determine to what extent compensatory hyperinsulinemia in mice with different genetic backgrounds and humans is driven by altered β-cell responsiveness to leptin.

These studies reveal that in the C57BL/6J mouse diet has a potent and pervasive effect on the health of the metabolic, skeletal, and neurological systems. Most of these defects represent

some of the most common defects observed with age in humans, such as loss of bone structure and cognitive decline. However, diet did not appear to accelerate general aging because the age-dependent decline in telomere was unaltered in HFHSD-fed mice. This gives rise to the possibility that many of these defects may represent the cumulative exposure to different toxic intermediates as a result of over-nutrition and may not be part of the aging process *per se*. One of the most surprising results observed here was the age-dependent resolution in glucose tolerance, which was concomitant with increased β-cell mass, increased circulating insulin, and a switch in β-cell responses to leptin. These studies give rise to a number of intriguing questions worthy of further investigation. Do all of these diseases have the same point of origin or do they occur independently? What other factors might work in concert with diet to increase the risk of certain defects preferentially over others? Do these defects arise from the diet itself or is this simply a consequence of a persistent state of positive energy balance that might be observed following overconsumption of any types of nutrients? Answering these questions will provide substantial advances to our understanding of the interaction between diet, obesity, and long-term health.

Experimental procedures

Animals

Male C57BL/6J mice (7 weeks old) were obtained from the Animal Resources Centre (Perth, Western Australia, Australia) and acclimatized for 1 week prior to experiments. Mice were maintained on a 12-h light/dark cycle (0700/1900 h) and given *ad libitum* access to food and water. Experiments were carried out in accordance with the National Health and Medical Research Council (Australia) guidelines for animal research and were approved by Garvan Institute/St. Vincent's Hospital and the University of Sydney Animal Experimentation Ethics Committees. To assess the effect of diet on overall health, we periodically measured changes in body weight, adipose tissue, muscle mass, glucose tolerance, insulin resistance, pancreatic β-cell function, bone, and neurological health in mice fed a HFHSD for up to 60 weeks. Most measurements were taken at 6, 24, and 60 weeks following initiation of diet. To ensure that data were not biased by cage to cage variability, studies were performed in multiple cohorts at two institutes. Data presented are a minimum of eight mice. Furthermore, individual cohorts were split into two groups so that glucose tolerance testing and sacrifice could be carried out within a 2-h period.

Experimental diets

Age-matched mice were maintained on either a standard laboratory chow (13% calories from fat, 65% carbohydrate, 22% protein from Gordon's Specialty Stock Feeds, Yanderra, New South Wales, Australia) or HFHSD (47% fat (7:1 lard-to-safflower oil ratio), 32% carbohydrate, 21% protein) and water. Food intake was measured cumulatively over 5 days by measuring the weight of the food before and after the allocated time, minus spillage. To calculate energy consumption, the weight of food consumed was multiplied by the diet energy density.

Body composition and mouse activity

Body composition was determined using dual-energy X-ray absorptiometry (DEXA) (Lunar PIXImus2 densitometer; GE Healthcare) in accordance with the manufacturer's instructions. Oxygen consumption rate (VO_2) and RER were measured under a consistent environmental temperature (22 °C) using an indirect calorimetry system (Oxymax series, Columbus Instruments). For mice, studies were commenced after 2 h of acclimation to the metabolic chamber using an air flow of 0.6 liters/min. VO_2 was measured in individual mice at 27-min intervals over a 24-h period. During the studies, chow and HFHSD mice had *ad libitum* access to food and water. Activity was quantified as the total number of beam breaks that occurred per 24 h while housed in the calorimetry chamber.

Tissue glycerol content as a measure of tissue triglycerides

Frozen tissue was powdered, and lipids were extracted using a standard chloroform/ methanol procedure. Triglyceride content was determined using an enzymatic colorimetric assay kit following the manufacturer's instructions (triglycerides GPO-PAP; Roche Diagnostics).

Bone health measures

Left and right femora were fixed in 4% paraformaldehyde for 16 h and then transferred to 70% ethanol. Femoral length was measured using calipers (Mitutoyo America). Femoral BMC and BMD were measured using the DEXA (Lunar PIXImus2 densitometer; GE Healthcare). The distal end of the right femur was scanned using μCT with a Skyscan 1172 scanner and associated analysis software (Skyscan) (50). Femoral images were captured at a resolution of 4.37 μm. The trabecular region of interest (ROI) was defined as 100–800 μm from the growth plate (9). The following parameters were generated: total bone volume, trabecular bone volume, trabecular bone thickness, trabecular number, and trabecular separation. For cortical bone volume and thickness, the ROI was defined as 2500–3500 μm from the growth plate. Endosteal and periosteal perimeters were traced and measured from the uppermost slice of the cortical ROI (3500 μm from the growth plate) and the average, γ, maximum, and polar moment of inertia (an index of bending strength) was calculated. All data were generated using CT-Analyzer software (Skyscan).

Telomere length assay

To obtain white blood cells, EDTA-anticoagulated blood taken from cardiac puncture (typically 600–1000 μl) was centrifuged at 1500 × *g* for 15 min at 4 °C. The white blood cell layer was isolated, and DNA was extracted using DNeasy blood and tissue kit from Qiagen following the manufacturer's instructions. DNA was quantified using SYBR Green (Life Technologies, Inc.). Telomere length was quantified by qPCR, using primers for the telomeric sequence and genomic control 36B4 as described previously (51). 10 ng of genomic DNA was amplified in 10-μl reactions using 0.25 μM forward and reverse primers, using the Universal FastStart SYBR Green qPCR kit (Roche Diagnostics) in a 384-well plate format with the Roche LightCycler480 instrument. Cycling conditions included an

initial 10-min denaturation step at 95 °C, followed by 40 cycles of 15 s at 95 °C and 1 min at 60 °C, and concluded with a melting curve between 60 and 95 °C. Serial dilutions of pooled samples were used to assess PCR efficiency and to generate standard curves for quantifying relative telomere and 36B4 levels. Telomere levels were normalized to 36B4 levels to obtain relative telomere length.

Amyloid β40 and β42 measurements

Brain tissue was carefully dissected from the skull, snap-frozen, and stored at −80 °C until use. Hippocampi from chow- and HFD-fed mice were weighed and homogenized in 5 M guanidine HCl, 50 mM Tris-HCl and further diluted in BSA and Tris-supplemented Dulbecco's PBS (BSAT/DPBS) containing a protease mixture inhibitor. The supernatant was collected for the soluble Aβ ELISA. The Aβ levels were determined by using the commercially available ELISA kits (mouse Aβ42-KMB3441 and mouse Aβ40-KMB3481, Invitrogen). Total protein was quantified using the Bradford reagent and Aβ40 and Aβ42 levels were normalized appropriately.

Behavioral measurements

Open Field—The Open Field test was conducted as described previously (52). The open field test arena (40 × 40 cm) was situated in a large box with clear Plexiglas walls, no ceiling, and a white floor. Each chamber was set inside a larger sound-attenuating cubicle with lights illuminating the arena and a fan to eliminate background noise. Mice were placed into the center of the arena and allowed to explore the test box for 10 min, while a computer software program (Activity Monitor; Med Associates) recorded activity via photo beam detection inside the testing chambers. The total distance traveled over the course of the 10 min was recorded as a measure of general activity levels. The arena was cleaned with 70% EtOH between each mouse.

Elevated plus maze—The elevated plus maze was performed as described previously (52). The elevated plus maze consists of four arms (77 × 10 cm) elevated (70 cm) above the floor. Two of the arms contained 15-cm-high walls (enclosed arms), and the other two consisted of no walls (open arms). Each mouse was placed in the middle of the maze facing a closed arm and allowed to explore the maze for 5 min. A video camera recorded the mouse, and a computer software program (Limelight, Med Associates) was used to measure the time spent in the open arms, as an indication of anxiety-like behavior. The maze was cleaned with 70% EtOH between each mouse.

Y-maze—The Y-maze was performed as per Heneka *et al.* (53), with modification. Testing was conducted in an opaque Plexiglas Y maze consisting of three arms (40 × 4 × 17 cm high) diverging at a 120° angle. Each mouse was placed in the center of the Y-maze and allowed to explore freely through the maze during a 5-min session. The sequence and total number of arms entered were recorded. Arm entry was only counted when all four paws of the mouse were in the arm. Visits to each of the three arms consecutively was considered a triad. Percentage alternation was calculated as the number of triads divided by the maximum possible alternations (the total number of arms entered minus 2) × 100. The maze was cleaned between each mouse with 70% EtOH.

Glucose tolerance testing (glucose, insulin, and C-peptide measurements)

For the majority of glucose tolerance tests, mice were fasted for 6 h beginning at 0800 h, before administration of an intraperitoneal injection of a 10% glucose solution to achieve a final dose of 1 g/kg of fat-free mass. For experience to measure insulin clearance by assessing circulating insulin and C-peptide (Fig. 5, *G–I*), mice where fasted for 16 h overnight. Blood glucose was measured at time points indicated in whole blood sampled from the tail tip using an Accu-Check II glucometer (Roche Diagnostics) Blood samples were obtained via tail tip at 0, 15, 30, 60, 90, and 120 min, using 5-μl heparinized hematocrit tubes (Drummond) and ejecting samples into a mouse ultrasensitive insulin ELISA (90080, Crystal Chem) or C-peptide ELISA (90050, Crystal Chem). Postprandial measurements were taken at 0700 h, and fasting measurements were taken prior to the GTT at 1400 h.

In vitro glucose uptake in adipose

Epididymal adipose depots were removed from mice and immediately incubated in DMEM supplemented with 2% BSA and 20 mM HEPES, pH 7.4, at 37 °C. Visible non-parenchymal tissue was then removed, and explants were minced into fine pieces. Minced explants were washed twice and incubated in DMEM supplemented with 2% BSA and 20 mM HEPES, pH 7.4, for 2 h. Adipose explants were washed in modified Krebs-Ringer phosphate buffer (54) supplemented with 2% BSA, before stimulation with 0.5 or 10 nM insulin for 20 min where indicated at 37 °C. During the final 5 min, 50 μM unlabeled 2-deoxyglucose (2-DOG) containing 1 μCi/ml of 2-[^{3}H]DOG and 0.14 μCi/ml [^{14}C]mannitol was added (total volume 0.5 ml). Glucose/tracer uptake was stopped with three washes in ice-cold PBS, quantified by liquid scintillation spectroscopy, and corrected for extracellular [^{14}C]mannitol and protein content (55–57).

In vitro glucose uptake in muscle

Extensor digitorum longus (EDL) and soleus muscles were excised, mounted, and preincubated for 30 min at 30 °C in Krebs-Henseleit buffer containing 5.5 mM glucose, 2 mM pyruvate, and 0.1% BSA (KRH) (58). KRH was gassed with carbogen (95% O_2/5% CO_2). Glucose uptake was assessed in KRH containing 0.375 μCi/ml 2-[^{3}H]DOG and 0.05 μCi/ml [^{14}C]mannitol in a final volume of 2 ml for 20 min at 30 °C, with or without 100 nM insulin before muscles were washed in ice-cold PBS and snap-frozen. Frozen muscles were incubated in 1 M potassium hydroxide at 70 °C for 20 min. Tracer content was quantified by liquid scintillation spectroscopy (Beckman LS6500 counter), and cellular glucose uptake was calculated after correcting the 2-[^{3}H]DOG counts for extracellular [^{14}C]mannitol counts and tissue weight (55, 57).

Isolation of mouse pancreatic islets

Islets were isolated using collagenase/thermolysin digestion and handpicking under a stereomicroscope as described (57,

59) with modification. Briefly, 0.25 mg/ml Liberase (Sigma) in Hanks' balanced salt solution (GIBCO) with 20 mM HEPES was injected into the common bile duct. The pancreas was removed and incubated at 37 °C in a shaking water bath for 13 min. After two washes, the digested pancreas was passed through a 1000-mm mesh and subjected to a Histopaque 1119 and 1077 (Sigma) gradient. As a final purification, islets were hand-picked in HEPES Krebs-Ringer buffer (KRBH) (20 mM HEPES, pH 7.4; 119 mM NaCl; 4.75 mM KCl; 2.54 mM $CaCl_2$; 1.2 mM $MgSO_4$; 1.18 mM KH_2PO_4; 5 mM $NaHCO_3$) containing 5 mM glucose and 1 mg/ml BSA. Hand-picked islets were then recovered in RPMI 1640 media supplemented with 11 mM glucose and 10% FBS for 1 h before insulin secretion was assessed.

Islet insulin secretion

Islet static insulin secretion assays were performed as described previously (59) with the following modifications. After recovery, islets were transferred into KRBH containing 2.8 mM glucose and preincubated at 37 °C for 1 h. At the end of the preincubation, five islets of equivalent size were placed in KRBH supplemented with 2.8 or 16.7 mM glucose in the presence or absence of 20 ng/ml leptin for 1 h. The tubes were centrifuged at 1500 rpm for 5 min, and the islet incubation media were collected and frozen for insulin determination by an ELISA (Crystal Chem). The islet pellet was sonicated in 50 μl of lysis buffer (100 mM Tris, 300 mM NaCl, 10 mM NaF, 2 mM sodium orthovanadate) for determination of DNA concentration (Quant-iT Picogreen DNA kit, Thermo Fisher Scientific) and total insulin content (ELISA, Crystal Chem) of the islets. Insulin secretion and insulin content data are expressed relative to DNA content.

Pancreatic immunohistochemistry

Pancreata were removed, cleared of fat and lymph nodes, and fixed in 10% buffered formalin, transferred to 70% EtOH, embedded in paraffin, serially sectioned (5-μm sections), and mounted on Superfrost Plus slides (Thermo Fisher Scientific, Pittsburgh, PA). Slides were rehydrated and then transferred to water. Antigen retrieval was performed by submerging slides in the Target Retrieval solution (Dako, S1699) and heating to 125 °C for 1 min and 95 °C for 10 s before being cooled. Slides were placed in blocking solution (PBS containing 2% BSA, 5% goat, and 5% donkey serum (Sigma)) for 30 min at room temperature and then incubated in a primary antibody solution (blocking solution + 1° antibody) containing 1° antibody overnight at 4 °C. The following day slides were washed three times with T-TBS (0.1% Tween) followed by a 1-h incubation at room temperature in secondary antibody solution (PBS + 2% BSA (Sigma) + 2° antibody). Anti-insulin (catalog no. I8510) and anti-glucagon (catalog no. G2654) antibodies were from Sigma, and anti-Ki67 (RM-9106-S0) antibodies and DAPI were from Thermo Fisher Scientific. We quantified 3–4 pancreata per diet at each time point using three sections at least 150 μm apart from each other. Whole sections were imaged and stitched on a Leica DM6000 Power Mosaic using a ×40 PLAN APO objective. Image analysis was performed using custom image analysis pipelines deployed across the ilastik (60), Fiji (61), and WEKA (62) platforms. For gross measurements of pancreas, islet, and adipose tissues, classifiers generated using ilastik were used to generate pixel-based probability maps for features of interest. These were segmented and measured in Fiji using a series of custom macros; the primary segmentation was cleaned with a second round of machine learning, prior to final analysis. Nuclei and Ki-67 were segmented and counted in previously detected islets using custom macros. In total, we imaged and analyzed 3567 mm^2 of pancreas tissue in which we detected 11,001 islets that contained 294,158 nuclei.

Statistics

Data analysis was carried out using Prism 6 software (version 6.01). Statistical significance was set at $p < 0.05$. p values were calculated by the Mann-Whitney test, Wilcoxon signed-rank test, where indicated. Where appropriate, sub-groups were initially compared by two-way analysis of variance. If row or column factors were significant, specific sub-groups were then compared using Student's t test (adjusting for multiple comparisons using the Sidak method). Data are expressed as mean ± S.E. of the replicates. All glucose tolerance area under the curve calculations were performed in Prism 6 software (version 6.01) and were corrected for baseline.

Author contributions—J. G. B., C. C. M., K. L. H., J. C., G. J. C., D. E. J., and D. J. F. conceptualization; J. G. B. software; J. G. B., M. A. K., C. C. M., and D. J. F. formal analysis; J. G. B., M. A. K., J. S., B. V., T. J. B., P. A. B., J. C., D. E. J., and D. J. F. supervision; J. G. B., M. A. K., and D. J. F. validation; J. G. B., M. A. K., C. C. M., J. S., P. T. W., A. L. W., N. J. H., A. Y. M., X. M., J. R. K., M. E. N., S.-X. T., B. Y., K. C. T., N. K. W., E.-C. K., R. F. E., P. A. B., K. L. H., J. C., G. J. C., and D. J. F. investigation; J. G. B., M. A. K., and D. J. F. visualization; J. G. B., M. A. K., C. C. M., J. R. K., K. C. T., P. A. B., J. C., G. J. C., and D. J. F. methodology; J. G. B., M. A. K., C. C. M., D. E. J., and D. J. F. writing-original draft; J. G. B., M. A. K., C. C. M., J. S., P. T. W., A. L. W., N. J. H., A. Y. M., X. M., J. R. K., M. E. N., S.-X. T., B. Y., K. C. T., N. K. W., E.-C. K., R. F. E., B. V., T. J. B., P. A. B., K. L. H., J. C., G. J. C., D. E. J., and D. J. F. writing-review and editing; M. A. K., C. C. M., and D. J. F. data curation; C. C. M., K. C. T., and D. J. F. project administration; B. V., P. A. B., and D. E. J. resources; D. E. J. funding acquisition.

Acknowledgments—We thank members of the James laboratory for critical feedback. We thank technical staff in the Histopathology and Biological Testing Facility at the Garvan Institute and the Laboratory Animal Service Facility at the Charles Perkins Centre, University of Sydney.

References

1. Reaven, G. (2004) The metabolic syndrome or the insulin resistance syndrome? Different names, different concepts, and different goals. *Endocrinol. Metab. Clin. North Am.* **33**, 283–303 CrossRef Medline
2. Buettner, R., Schölmerich, J., and Bollheimer, L. C. (2007) High-fat diets: modeling the metabolic disorders of human obesity in rodents. *Obesity* **15**, 798–808 CrossRef Medline
3. Solon-Biet, S. M., McMahon, A. C., Ballard, J. W., Ruohonen, K., Wu, L. E., Cogger, V. C., Warren, A., Huang, X., Pichaud, N., Melvin, R. G., Gokarn, R., Khalil, M., Turner, N., Cooney, G. J., Sinclair, D. A., *et al.* (2014) The ratio of macronutrients, not caloric intake, dictates cardiometabolic health, aging, and longevity in *ad libitum*-fed mice. *Cell Metab.* **19**, 418–430 CrossRef Medline

4. Kahn, S. E., Hull, R. L., and Utzschneider, K. M. (2006) Mechanisms linking obesity to insulin resistance and type 2 diabetes. *Nature* **444**, 840–846 CrossRef Medline
5. Barclay, J. L., Shostak, A., Leliavski, A., Tsang, A. H., Jöhren, O., Müller-Fielitz, H., Landgraf, D., Naujokat, N., van der Horst, G. T., and Oster, H. (2013) High-fat diet-induced hyperinsulinemia and tissue-specific insulin resistance in Cry-deficient mice. *Am. J. Physiol. Endocrinol. Metab.* **304**, E1053–E1063 CrossRef Medline
6. Murphy, E. A., Velazquez, K. T., and Herbert, K. M. (2015) Influence of high-fat diet on gut microbiota: a driving force for chronic disease risk. *Curr. Opin. Clin. Nutr. Metab. Care* **18**, 515–520 CrossRef Medline
7. Wellen, K. E., and Hotamisligil, G. S. (2005) Inflammation, stress, and diabetes. *J. Clin. Invest.* **115**, 1111–1119 CrossRef Medline
8. Cao, J. J., Gregoire, B. R., and Gao, H. (2009) High-fat diet decreases cancellous bone mass but has no effect on cortical bone mass in the tibia in mice. *Bone* **44**, 1097–1104 CrossRef Medline
9. Cao, J. J., Sun, L., and Gao, H. (2010) Diet-induced obesity alters bone remodeling leading to decreased femoral trabecular bone mass in mice. *Ann. N. Y. Acad. Sci.* **1192**, 292–297 CrossRef Medline
10. Rosenkranz, S. K., Townsend, D. K., Steffens, S. E., and Harms, C. A. (2010) Effects of a high-fat meal on pulmonary function in healthy subjects. *Eur. J. Appl. Physiol.* **109**, 499–506 CrossRef Medline
11. Altunkaynak, M. E., Ozbek, E., Altunkaynak, B. Z., Can, I., Unal, D., and Unal, B. (2008) The effects of high-fat diet on the renal structure and morphometric parametric of kidneys in rats. *J. Anat.* **212**, 845–852 CrossRef Medline
12. Arvanitakis, Z., Wilson, R. S., Bienias, J. L., Evans, D. A., and Bennett, D. A. (2004) Diabetes mellitus and risk of Alzheimer disease and decline in cognitive function. *Arch. Neurol.* **61**, 661–666 CrossRef Medline
13. Dineley, K. T., Jahrling, J. B., and Denner, L. (2014) Insulin resistance in Alzheimer's disease. *Neurobiol. Dis.* **72,** 92–103 CrossRef Medline
14. Devlin, M. J., Van Vliet, M., Motyl, K., Karim, L., Brooks, D. J., Louis, L., Conlon, C., Rosen, C. J., and Bouxsein, M. L. (2014) Early-onset type 2 diabetes impairs skeletal acquisition in the male TALLYHO/JngJ mouse. *Endocrinology* **155**, 3806–3816 CrossRef Medline
15. Wongdee, K., and Charoenphandhu, N. (2015) Update on type 2 diabetes-related osteoporosis. *World J. Diabetes* **6**, 673–678 CrossRef Medline
16. Strachan, M. W. (2003) Insulin and cognitive function. *Lancet* **362**, 1253 CrossRef Medline
17. Ashe, K. H. (2001) Learning and memory in transgenic mice modeling Alzheimer's disease. *Learn. Mem.* **8**, 301–308 CrossRef Medline
18. Ballard, C., and Walker, M. (1999) Neuropsychiatric aspects of Alzheimer's disease. *Curr. Psychiatry Rep.* **1**, 49–60 Medline
19. Kieffer, T. J., Heller, R. S., Leech, C. A., Holz, G. G., and Habener, J. F. (1997) Leptin suppression of insulin secretion by the activation of ATP-sensitive K^+ channels in pancreatic beta-cells. *Diabetes* **46**, 1087–1093 Medline
20. Zhao, A. Z., Bornfeldt, K. E., and Beavo, J. A. (1998) Leptin inhibits insulin secretion by activation of phosphodiesterase 3B. *J. Clin. Invest.* **102**, 869–873 CrossRef Medline
21. Morioka, T., Asilmaz, E., Hu, J., Dishinger, J. F., Kurpad, A. J., Elias, C. F., Li, H., Elmquist, J. K., Kennedy, R. T., and Kulkarni, R. N. (2007) Disruption of leptin receptor expression in the pancreas directly affects beta cell growth and function in mice. *J. Clin. Invest.* **117**, 2860–2868 CrossRef Medline
22. Toye, A. A., Lippiat, J. D., Proks, P., Shimomura, K., Bentley, L., Hugill, A., Mijat, V., Goldsworthy, M., Moir, L., Haynes, A., Quarterman, J., Freeman, H. C., Ashcroft, F. M., and Cox, R. D. (2005) A genetic and physiological study of impaired glucose homeostasis control in C57BL/6J mice. *Diabetologia* **48**, 675–686 CrossRef Medline
23. Turner, N., Kowalski, G. M., Leslie, S. J., Risis, S., Yang, C., Lee-Young, R. S., Babb, J. R., Meikle, P. J., Lancaster, G. I., Henstridge, D. C., White, P. J., Kraegen, E. W., Marette, A., Cooney, G. J., Febbraio, M. A., and Bruce, C. R. (2013) Distinct patterns of tissue-specific lipid accumulation during the induction of insulin resistance in mice by high-fat feeding. *Diabetologia* **56**, 1638–1648 CrossRef Medline
24. Park, S. Y., Cho, Y. R., Kim, H. J., Higashimori, T., Danton, C., Lee, M. K., Dey, A., Rothermel, B., Kim, Y. B., Kalinowski, A., Russell, K. S., and Kim, J. K. (2005) Unraveling the temporal pattern of diet-induced insulin resistance in individual organs and cardiac dysfunction in C57BL/6 mice. *Diabetes* **54**, 3530–3540 CrossRef Medline
25. Kowalski, G. M., Kraakman, M. J., Mason, S. A., Murphy, A. J., and Bruce, C. R. (2017) Resolution of glucose intolerance in long-term high-fat, high-sucrose-fed mice. *J. Endocrinol.* **233**, 269–279 CrossRef Medline
26. Wong, N., Blair, A. R., Morahan, G., and Andrikopoulos, S. (2010) The deletion variant of nicotinamide nucleotide transhydrogenase (Nnt) does not affect insulin secretion or glucose tolerance. *Endocrinology* **151**, 96–102 CrossRef Medline
27. Hamrick, M. W., Pennington, C., Newton, D., Xie, D., and Isales, C. (2004) Leptin deficiency produces contrasting phenotypes in bones of the limb and spine. *Bone* **34**, 376–383 CrossRef Medline
28. Wauman, J., and Tavernier, J. (2011) Leptin receptor signaling: pathways to leptin resistance. *Front. Biosci.* **16**, 2771–2793 Medline
29. Klein, G. L. (2014) Insulin and bone: recent developments. *World J. Diabetes* **5**, 14–16 CrossRef Medline
30. de la Mata, J., Uy, H. L., Guise, T. A., Story, B., Boyce, B. F., Mundy, G. R., and Roodman, G. D. (1995) Interleukin-6 enhances hypercalcemia and bone resorption mediated by parathyroid hormone-related protein *in vivo*. *J. Clin. Invest.* **95**, 2846–2852 CrossRef Medline
31. Oftadeh, R., Perez-Viloria, M., Villa-Camacho, J. C., Vaziri, A., and Nazarian, A. (2015) Biomechanics and mechanobiology of trabecular bone: a review. *J. Biomech. Eng.* **137**, 10.1115/1.4029176 CrossRef Medline
32. Hamrick, M. W. (2007) Leptin and bone: a consensus emerging? *Bone KEy-Osteovision* **4**, 99–107
33. Ducy, P., Amling, M., Takeda, S., Priemel, M., Schilling, A. F., Beil, F. T., Shen, J., Vinson, C., Rueger, J. M., and Karsenty, G. (2000) Leptin inhibits bone formation through a hypothalamic relay: a central control of bone mass. *Cell* **100**, 197–207 CrossRef Medline
34. Craft, S., Peskind, E., Schwartz, M. W., Schellenberg, G. D., Raskind, M., and Porte, D., Jr. (1998) Cerebrospinal fluid and plasma insulin levels in Alzheimer's disease: relationship to severity of dementia and apolipoprotein E genotype. *Neurology* **50**, 164–168 CrossRef Medline
35. van Himbergen, T. M., Beiser, A. S., Ai, M., Seshadri, S., Otokozawa, S., Au, R., Thongtang, N., Wolf, P. A., and Schaefer, E. J. (2012) Biomarkers for insulin resistance and inflammation and the risk for all-cause dementia and Alzheimer disease: results from the Framingham Heart Study. *Arch. Neurol.* **69**, 594–600 CrossRef Medline
36. Talbot, K., Wang, H. Y., Kazi, H., Han, L. Y., Bakshi, K. P., Stucky, A., Fuino, R. L., Kawaguchi, K. R., Samoyedny, A. J., Wilson, R. S., Arvanitakis, Z., Schneider, J. A., Wolf, B. A., Bennett, D. A., Trojanowski, J. Q., and Arnold, S. E. (2012) Demonstrated brain insulin resistance in Alzheimer's disease patients is associated with IGF-1 resistance, IRS-1 dysregulation, and cognitive decline. *J. Clin. Invest.* **122**, 1316–1338 CrossRef Medline
37. Xu, H., Barnes, G. T., Yang, Q., Tan, G., Yang, D., Chou, C. J., Sole, J., Nichols, A., Ross, J. S., Tartaglia, L. A., and Chen, H. (2003) Chronic inflammation in fat plays a crucial role in the development of obesity-related insulin resistance. *J. Clin. Invest.* **112**, 1821–1830 CrossRef Medline
38. Lee, Y. S., Li, P., Huh, J. Y., Hwang, I. J., Lu, M., Kim, J. I., Ham, M., Talukdar, S., Chen, A., Lu, W. J., Bandyopadhyay, G. K., Schwendener, R., Olefsky, J., and Kim, J. B. (2011) Inflammation is necessary for long-term but not short-term high-fat diet-induced insulin resistance. *Diabetes* **60**, 2474–2483 CrossRef Medline
39. Steil, G. M., Trivedi, N., Jonas, J. C., Hasenkamp, W. M., Sharma, A., Bonner-Weir, S., and Weir, G. C. (2001) Adaptation of beta-cell mass to substrate oversupply: enhanced function with normal gene expression. *Am. J. Physiol. Endocrinol. Metab.* **280**, E788–E796 CrossRef Medline
40. Jetton, T. L., Lausier, J., LaRock, K., Trotman, W. E., Larmie, B., Habibovic, A., Peshavaria, M., and Leahy, J. L. (2005) Mechanisms of compensatory beta-cell growth in insulin-resistant rats: roles of Akt kinase. *Diabetes* **54**, 2294–2304 CrossRef Medline
41. Liu, Y. Q., Jetton, T. L., and Leahy, J. L. (2002) beta-Cell adaptation to insulin resistance. Increased pyruvate carboxylase and malate-pyruvate shuttle activity in islets of nondiabetic Zucker fatty rats. *J. Biol. Chem.* **277**, 39163–39168 CrossRef Medline
42. Chen, C., Hosokawa, H., Bumbalo, L. M., and Leahy, J. L. (1994) Mechanism of compensatory hyperinsulinemia in normoglycemic insulin-resist-

ant spontaneously hypertensive rats. Augmented enzymatic activity of glucokinase in beta-cells. *J. Clin. Invest.* **94**, 399–404 CrossRef Medline
43. Baquero, A. F., de Solis, A. J., Lindsley, S. R., Kirigiti, M. A., Smith, M. S., Cowley, M. A., Zeltser, L. M., and Grove, K. L. (2014) Developmental switch of leptin signaling in arcuate nucleus neurons. *J. Neurosci.* **34**, 9982–9994 CrossRef Medline
44. Covey, S. D., Wideman, R. D., McDonald, C., Unniappan, S., Huynh, F., Asadi, A., Speck, M., Webber, T., Chua, S. C., and Kieffer, T. J. (2006) The pancreatic beta cell is a key site for mediating the effects of leptin on glucose homeostasis. *Cell Metab.* **4**, 291–302 CrossRef Medline
45. Niswender, K. D., and Magnuson, M. A. (2007) Obesity and the beta cell: lessons from leptin. *J. Clin. Invest.* **117**, 2753–2756 CrossRef Medline
46. Wu, L. E., Samocha-Bonet, D., Whitworth, P. T., Fazakerley, D. J., Turner, N., Biden, T. J., James, D. E., and Cantley, J. (2014) Identification of fatty acid binding protein 4 as an adipokine that regulates insulin secretion during obesity. *Mol. Metab.* **3**, 465–473 CrossRef Medline
47. Vaag, A., Damsbo, P., Hother-Nielsen, O., and Beck-Nielsen, H. (1992) Hyperglycaemia compensates for the defects in insulin-mediated glucose metabolism and in the activation of glycogen synthase in the skeletal muscle of patients with type 2 (non-insulin-dependent) diabetes mellitus. *Diabetologia* **35**, 80–88 CrossRef Medline
48. Groop, L. (2000) Pathogenesis of type 2 diabetes: the relative contribution of insulin resistance and impaired insulin secretion. *Int. J. Clin. Pract. Suppl.* **2000,** 3–13 Medline
49. Stöckli, J., Fisher-Wellman, K. H., Chaudhuri, R., Zeng, X. Y., Fazakerley, D. J., Meoli, C. C., Thomas, K. C., Hoffman, N. J., Mangiafico, S. P., Xirouchaki, C. E., Yang, C. H., Ilkayeva, O., Wong, K., Cooney, G. J., Andrikopoulos, S., *et al.* (2017) Metabolomic analysis of insulin resistance across different mouse strains and diets. *J. Biol. Chem.* **292**, 19135–19145 CrossRef Medline
50. Wong, I. P., Nguyen, A. D., Khor, E. C., Enriquez, R. F., Eisman, J. A., Sainsbury, A., Herzog, H., and Baldock, P. A. (2013) Neuropeptide Y is a critical modulator of leptin's regulation of cortical bone. *J. Bone Miner. Res.* **28**, 886–898 CrossRef Medline
51. Cawthon, R. M. (2002) Telomere measurement by quantitative PCR. *Nucleic Acids Res* **30**, e47 CrossRef Medline
52. Wright, A. L., Zinn, R., Hohensinn, B., Konen, L. M., Beynon, S. B., Tan, R. P., Clark, I. A., Abdipranoto, A., and Vissel, B. (2013) Neuroinflammation and neuronal loss precede Aβ plaque deposition in the hAPP-J20 mouse model of Alzheimer's disease. *PLoS One* **8**, e59586 CrossRef Medline
53. Heneka, M. T., Kummer, M. P., Stutz, A., Delekate, A., Schwartz, S., Vieira-Saecker, A., Griep, A., Axt, D., Remus, A., Tzeng, T. C., Gelpi, E., Halle, A., Korte, M., Latz, E., and Golenbock, D. T. (2013) NLRP3 is activated in Alzheimer's disease and contributes to pathology in APP/PS1 mice. *Nature* **493**, 674–678 Medline
54. Burchfield, J. G., Lu, J., Fazakerley, D. J., Tan, S. X., Ng, Y., Mele, K., Buckley, M. J., Han, W., Hughes, W. E., and James, D. E. (2013) Novel systems for dynamically assessing insulin action in live cells reveals heterogeneity in the insulin response. *Traffic* **14**, 259–273 CrossRef Medline
55. Stöckli, J., Meoli, C. C., Hoffman, N. J., Fazakerley, D. J., Pant, H., Cleasby, M. E., Ma, X., Kleinert, M., Brandon, A. E., Lopez, J. A., Cooney, G. J., and James, D. E. (2015) The RabGAP TBC1D1 plays a central role in exercise-regulated glucose metabolism in skeletal muscle. *Diabetes* **64**, 1914–1922 CrossRef Medline
56. Tan, S. X., Fisher-Wellman, K. H., Fazakerley, D. J., Ng, Y., Pant, H., Li, J., Meoli, C. C., Coster, A. C., Stöckli, J., and James, D. E. (2015) Selective insulin resistance in adipocytes. *J. Biol. Chem.* **290**, 11337–11348 CrossRef Medline
57. Li, J., Cantley, J., Burchfield, J. G., Meoli, C. C., Stöckli, J., Whitworth, P. T., Pant, H., Chaudhuri, R., Groffen, A. J., Verhage, M., and James, D. E. (2014) DOC2 isoforms play dual roles in insulin secretion and insulin-stimulated glucose uptake. *Diabetologia* **57**, 2173–2182 CrossRef Medline
58. Aslesen, R., Engebretsen, E. M., Franch, J., and Jensen, J. (2001) Glucose uptake and metabolic stress in rat muscles stimulated electrically with different protocols. *J. Appl. Physiol.* **91**, 1237–1244 CrossRef Medline
59. Kebede, M. A., Oler, A. T., Gregg, T., Balloon, A. J., Johnson, A., Mitok, K., Rabaglia, M., Schueler, K., Stapleton, D., Thorstenson, C., Wrighton, L., Floyd, B. J., Richards, O., Raines, S., Eliceiri, K., *et al.* (2014) SORCS1 is necessary for normal insulin secretory granule biogenesis in metabolically stressed beta cells. *J. Clin. Invest.* **124**, 4240–4256 CrossRef Medline
60. Sommer, C., Straehle, C., Kothe, U., and Hampreht, F, A. (2011) *2011 IEEE International Symposium on Biomedical Imaging: From Nano to Macro (ISBI), 3/30–4/2/2011, Chicago, IL,* Abstr. 230–233, IEEE, New York CrossRef
61. Schindelin, J., Arganda-Carreras, I., Frise, E., Kaynig, V., Longair, M., Pietzsch, T., Preibisch, S., Rueden, C., Saalfeld, S., Schmid, B., Tinevez, J. Y., White, D. J., Hartenstein, V., Eliceiri, K., Tomancak, P., and Cardona, A. (2012) Fiji: an open-source platform for biological-image analysis. *Nat. Methods* **9**, 676–682 CrossRef Medline
62. Hall, M., Frank, E., Holmes, G., Pfahringer, B., Reutemann, P., and Witten, I. (2009) The WEKA data mining software: an update. *SIGKDD Explor. Newsl.* **11**, 10–18 CrossRef

High dietary fat and sucrose result in an extensive and time-dependent deterioration in health of multiple physiological systems in mice

James G. Burchfield, Melkam A. Kebede, Christopher C. Meoli, Jacqueline Stöckli, P. Tess Whitworth, Amanda L. Wright, Nolan J. Hoffman, Annabel Y. Minard, Xiuquan Ma, James R. Krycer, Marin E. Nelson, Shi-Xiong Tan, Belinda Yau, Kristen C. Thomas, Natalie K. Y. Wee, Ee-Cheng Khor, Ronaldo F. Enriquez, Bryce Vissel, Trevor J. Biden, Paul A. Baldock, Kyle L. Hoehn, James Cantley, Gregory J. Cooney, David E. James and Daniel J. Fazakerley

J. Biol. Chem. 2018, 293:5731-5745.
doi: 10.1074/jbc.RA117.000808 originally published online February 13, 2018